THE JOURNAL OF BIOLOGICAL CHEMISTRY
Vol. 279, No. 10, Issue of March 5, pp. 9353–9361, 2004

Printed in U.S.A.

X-ray Crystallographic and Site-directed Mutagenesis Analysis of the Mechanism of Schiff-base Formation in Phosphonoacetaldehyde Hydrolase Catalysis*

Received for publication, November 11, 2003
Published, JBC Papers in Press, December 10, 2003, DOI 10.1074/jbc.M312345200

Marc C. Morais‡, Guofeng Zhang§, Wenhai Zhang§, David B. Olsen§¶, Debra Dunaway-Mariano§‖, and Karen N. Allen‡**

From the ‡Department of Physiology and Biophysics, Boston University School of Medicine, Boston, Massachusetts 02118-2394 and the §Department of Chemistry, University of New Mexico, Albuquerque, New Mexico 87131

Phosphonoacetaldehyde hydrolase (phosphonatase) catalyzes the hydrolytic P–C bond cleavage of phosphonoacetaldehyde (Pald) to form orthophosphate and acetaldehyde. The reaction proceeds via a Schiff-base intermediate formed between Lys-53 and the Pald carbonyl. The x-ray crystal structures of the wild-type phosphonatase complexed with Mg(II) alone or with Mg(II) plus vinylsulfonate (a phosphonoethylenamine analog) were determined to 2.8 and 2.4 Å, respectively. These structures were used to determine the identity and positions of active site residues surrounding the Lys-53 ammonium group and the Pald carbonyl. These include Cys-22, His-56, Tyr-128, and Met-49. Site-directed mutagenesis was then employed to determine whether or not these groups participate in catalysis. Based on rate contributions, Tyr-128 and Cys-22 were eliminated as potential catalytic groups. The Lys-53 ϵ-amino group, positioned for reaction with the Pald carbonyl, forms a hydrogen bond with water 120. Water 120 is also within hydrogen bond distance of an imidazole nitrogen of His-56 and the sulfur atom of Met-49. Kinetic constants for mutants indicated that His-56 (1000-fold reduction in k_{cat}/K_m upon Ala substitution) and Met-49 (17,000-fold reduction in k_{cat}/K_m upon Leu substitution) function in catalysis of Schiff-base formation. Based on these results, it is proposed that a network of hydrogen bonds among Lys-53, water 120, His-56, and Met-49 facilitate proton transfer from Lys-53 to the carbinolamine intermediate. Comparison of the vinylsulfonate complex *versus* unliganded structures indicated that association of the cap and core domains is essential for the positioning of the Lys-53 for attack at the Pald carbonyl and that substrate binding at the core domain stabilizes cap domain binding.

Naturally occurring phosphonates return to the phosphate pool via the action of P–C bond lyases or hydrolases (for a recent review see Ref. 1). Simple alkylphosphonates (*e.g.* methylphosphonate) are processed by homolytic P–C bond cleavage catalyzed by a membrane-associated multienzyme complex called "C–P lyase" (2). β-Carbonoalkylphosphonates, which contain polarized P–C bonds, undergo heterolytic bond cleavage reactions catalyzed by phosphonohydrolases. Known phosphonohydrolases include phosphonoacetate hydrolase (3), phosphonopyruvate hydrolase (4), and the topic of this paper, phosphonoacetaldehyde hydrolase (phosphonatase)[1] (5).

Phosphonatase catalyzes the dephosphonylation of phosphonoacetaldehyde (Pald) by using an active site amine (Lys-53) to convert the substrate aldehyde group to an iminium ion prior to P–C bond cleavage (Fig. 1). The leaving group is the low energy, Lys-53-Nϵ-ethylenamine. In earlier work, the Schiff-base formed between Lys-53 and the acetaldehyde product had been trapped and then identified by reduction of the iminium ion accumulated under steady-state conditions (6). Consistent with the role of the active site Lys-53 in Schiff-base formation, mutation to Arg resulted in total loss of catalytic activity (7).

Phosphonatase shares the use of electrophilic catalysis by Schiff-base formation with numerous C–C bond-cleaving enzymes including acetoacetate decarboxylase, transaldolase, and Class I aldolases (for review see Ref. 8). Model studies of amine *versus* enzyme (acetoacetate decarboxylase) catalyzed decarboxylation of acetoacetate have shown that Schiff-base formation with the enzyme active site amine is at least 1000-fold faster than with the solvated amine (8–11). The rate difference derives in part from the ability of the enzyme to shuttle protons to and from the reaction site.

As illustrated in Fig. 2, the solution reaction proceeds via the attack of the neutral amine on the reactant carbonyl carbon to form a dipolar intermediate (12). The proton moves from nitrogen to oxygen in the dipolar intermediate to form the neutral carbinolamine. The nonbonding electrons on the nitrogen of the carbinolamine serve to expel the hydroxide and form the protonated Schiff-base. In the enzyme active site, a proton can be removed from the Lys-Ne-ammonium group, facilitating nucleophilic attack on the substrate carbonyl, and further along the reaction pathway, a proton can be delivered to the carbinolamine hydroxyl group as it is expelled *en route* to Schiff-base formation.

The aim of this study was to determine whether such proton transfers occur in the phosphonatase catalytic mechanism,

* This work was supported by National Institutes of Health Grant GM61099 (to K. N. A. and D. D.-M.). The costs of publication of this article were defrayed in part by the payment of page charges. This article must therefore be hereby marked "*advertisement*" in accordance with 18 U.S.C. Section 1734 solely to indicate this fact.

The atomic coordinates and structure factors (codes 1RQN and 1RQL for the unliganded and vinylsulfonate-bound wild-type phosphonatase structures, respectively) have been deposited in the Protein Data Bank, Research Collaboratory for Structural Bioinformatics, Rutgers University, New Brunswick, NJ (http://www.rcsb.org/).

¶ Current address: Dept. of Biological Chemistry, Merck Research Laboratories, WP26-265, West Point, PA 19486.

‖ To whom correspondence may be addressed: Dept. of Chemistry, University of New Mexico, Albuquerque, NM 87131. Tel.: 505-277-3383; Fax: 505-277-6202; E-mail: dd39@unm.edu.

** To whom correspondence may be addressed: Dept. of Physiology and Biophysics, Boston University School of Medicine, 715 Albany St., Boston, MA 02118-2394. Tel.: 617-638-4398; Fax: 617-638-4273; E-mail: allen@med-xtal.bu.edu.

[1] The abbreviations used are: phosphonatase, phosphonoacetaldehyde hydrolase; Pald, phosphonoacetaldehyde; CNS, crystallography NMR software; vSO_3, vinyl sulfonate.

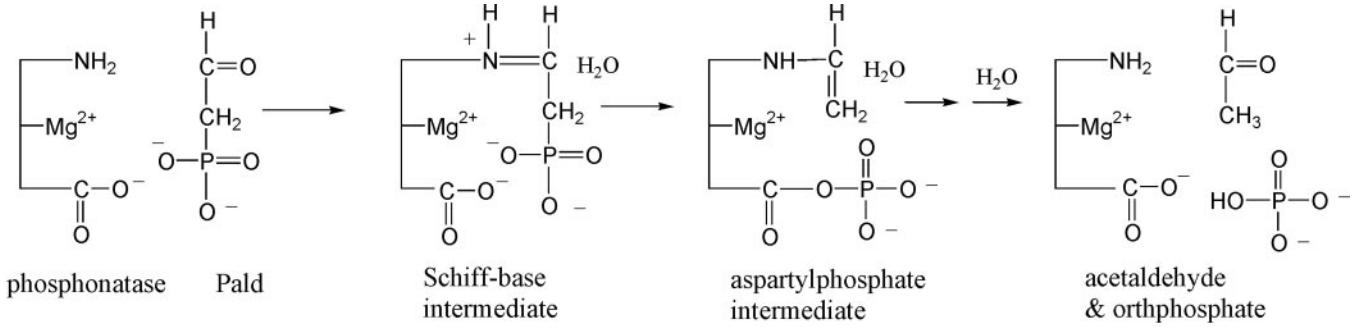

FIG. 1. **The reaction pathway of phosphonatase-catalyzed hydrolytic P–C bond cleavage of Pald.**

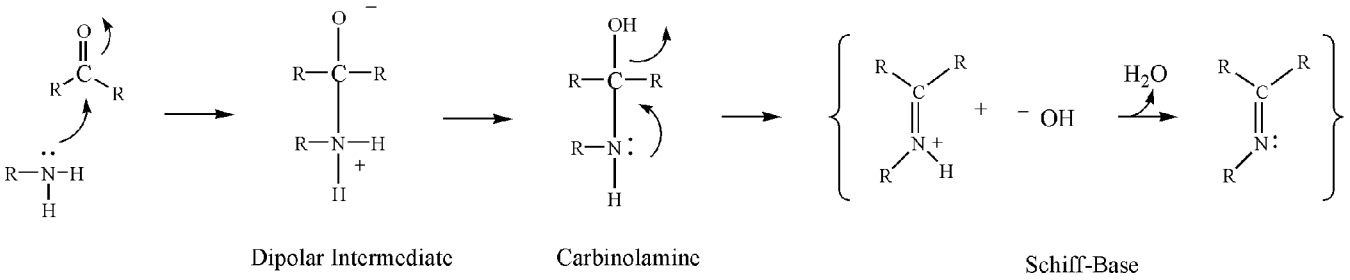

FIG. 2. **Mechanism of Schiff-base formation between an amine and a ketone in aqueous solution (12).**

first by determining the proximity of active site acid/base groups relative to the reaction center using x-ray crystallographic techniques. These residues were then evaluated as possible acid/base catalysts by replacing them via site-directed mutagenesis and measuring the catalytic efficiency of the mutant enzyme. In this paper, the results of the structure-function study are reported, and a mechanism for Schiff base formation in phosphonatase catalysis is proposed.

MATERIALS AND METHODS

Preparation of Wild-type and Mutant Phosphonatase—Pald was prepared according to the published procedure (13). The wild-type *Bacillus cereus* enzyme was prepared from the *Escherichia coli* clone as described previously (7, 14). The mutant genes were generated by polymerase chain reaction using the plasmid pKK223-3 containing the wild-type phosphonatase gene (7) as template. The C22A, C22S, M49L, H56A, Y128A, Y128F, and Y128F/C22S phosphonatase mutants were purified using the same procedure used to purify the wild-type enzyme (7) in yields of 10–20 mg/g cell paste. The chromatographic behavior, solubility, and stability to storage of the mutants were similar to those of the wild-type enzyme.

Steady-state Kinetic Constants—The K_m and V_{max} values for wild-type and mutant phosphonatases were determined from the initial velocity data measured as a function of Pald concentration (0.5–10 K_m). The 1-ml reaction solutions contained Pald, 10 mM $MgCl_2$, 0.15 mM NADH, and 5 units of alcohol dehydrogenase dissolved in 50 mM K^+-Hepes (pH 7.5, 25 °C). The concentration of phosphonatase used was in the range of 0.02 to 2.0 μM depending on the mutant studied. Reactions were monitored at 340 nm ($\Delta\epsilon$ = 6200 M^{-1} cm^{-1}) for the conversion of acetaldehyde and NADH to ethanol and NAD^+. The initial velocity data were analyzed using Equation 1,

$$V_o = V_{max}[A]/(K_m + [A]) \quad \text{(Eq. 1)}$$

where [A] is the substrate concentration, V_o is the initial velocity, V_{max} is the maximum velocity, and K_m is the Michaelis constant. The k_{cat} was calculated from V_{max} and the enzyme concentration using the equation $k_{cat} = V_{max}/[E]$. The enzyme concentration was determined using the Bradford method (15).

The K_i of vinylsulfonate (vSO_3) was determined by measuring the initial velocity of phosphonatase-catalyzed hydrolysis of Pald as a function of substrate concentration (25–300 μM) and vSO_3 concentration (0-, 2-, and 4-fold K_i). The K_i value was calculated from the initial velocity data by using the rate equation for competitive inhibition,

$$v = VS/[K_m(1 + I/K_i) + S] \quad \text{(Eq. 2)}$$

where v is the initial velocity, V is the maximal velocity, S is the concentration of the substrate, K_m is the Michaelis constant for the substrate, and I is the concentration of the inhibitor.

Crystallization and Data Collection—Wild-type phosphonatase was concentrated to 10 mg protein/ml in 1 mM K^+-Hepes, 10 mM $MgCl_2$, and 0.1 mM dithiothreitol (pH 7.5, 4 °C). Protein crystals were obtained by using the vapor diffusion method with hanging-drop geometry at 18 °C as described previously for crystallization of the wild-type enzyme (16) (*viz*. 10 μl each of protein solution and well solution consisting of 30% polyethylene glycol 4000, 100 mM Tris-HCl, pH 7.4, and 100 mM $MgCl_2$). Large (0.4 mm/side) crystals grew within a week. For the vSO_3-bound structure, 5 mM vSO_3 was added to the well solution during crystallization. Before data collection, crystals were soaked (1–12 h) in well solution plus 20% glycerol and frozen in a stream of nitrogen gas cooled by liquid nitrogen at −180 °C. Data were collected on beamline X12B at Brookhaven National Laboratory's National Synchrotron Light Source using a 60-mm MAR detector (to 2.8 Å resolution for the crystal of the phosphonatase-Mg(II) complex and to 2.4 Å for the phosphonatase-Mg(II)-vSO_3 complex.

The DENZO and SCALEPACK programs (17) were used for data indexing, reduction, and scaling. Crystals of both complexes were monoclinic and belong to space group C2. Crystals of the phosphonatase-Mg(II) complex had unit-cell dimensions of a = 210.13 Å, b = 45.18 Å, c = 63.64 Å, and β = 105.1°, and crystals of the phosphonatase-Mg(II)-vSO_3 complex were isomorphous, with unit-cell dimensions of a = 209.97 Å, b = 45.27 Å, c = 64.63 Å, and β = 104.9°. Assuming a Matthew's coefficient of 2.3, the unit-cell dimensions are consistent with a dimer in the asymmetric unit for both crystals (18).

Structure Solution and Refinement—The molecular replacement method was used to phase the data sets (19, 20). The 3.0 Å structure of the phosphonatase-Mg(II)-tungstate complex (Protein Data Bank accession code 1FEZ (14)), with tungstate and water molecules removed, was positioned in the C2 cell with the program AMoRE (20) using data between 10.0 and 4.2 Å. The previously solved structure showed that phosphonatase exists in an open and a closed conformation of the cap domain relative to the core domain, and therefore the search model comprised combinations of open and closed monomers. The dimer model corresponding to one "open" and one "closed" monomer resulted in the best initial AMoRE solution, as well as the lowest R-factor after rigid body refinement.

The initial molecular replacement solutions for the structures were subjected to one round of simulated annealing using slow-cool torsional molecular dynamics as implemented in CNS excluding 7% of the data for the calculation of R_{free} (21). Iterative cycles of minimization against the x-ray terms as implemented in CNS followed by manual rebuilding using the graphics program O (22) using $2F_o - F_c$ and $F_o - F_c$ maps

TABLE I
Data collection, refinement statistics, and stereochemical quality of the final models for phosphonatase bound to Mg(II) alone and to Mg(II) and vSO_3

	Mg(II) complex	Mg(II)-vSO_3 complex
Data collection statistics		
Resolution range (Å)	∞–2.8	∞–2.4
No. of unique reflections	13,003	20,810
Completeness (%)[a]	85.0(57.6)	96.7 (99.3)
$I/(\sigma(I))$[a]	8.5(2.01)	11.5(3.18)
R_{merge}[a,b] (%)	10.0(46.2)	8.7(36.0)
Refinement and model statistics		
No. of reflections used in refinement	12,399	17,343
Final R_{work}[c]	0.254	0.242
Final R_{free}[d]	0.287	0.274
Average B-value (Å^2)	54.4	36.0
Main chain	52.1	33.3
Side chain	56.3	38.7
r.m.s.d.[e] from ideality		
Bond lengths (Å)	0.009	0.009
Bond angles (degrees)	1.40	1.43
Dihedral angles (degrees)	20.96	21.69
B r.m.s.d.[e] for bonded atoms (Å^2)		
Main chain	8.4	4.5
Side chain	9.2	6.8
Estimated coordinate error (Å)	0.44	0.44

[a] Statistics for the outermost shell (2.95–2.80 and 2.36–2.40 for the unliganded and liganded phosphonatase) are given in parentheses.
[b] $R_{merge} = \Sigma_{hkl}\,\Sigma_i|I_{hkl,\,i} - \langle I_{hkl}\rangle\, I|\,/\,\Sigma_{hkl}\,\Sigma_{\,i}|I_{hkl,\,i}|$, where $\langle I_{hkl}\rangle$ is the mean intensity of the multiple $I_{hkl,\,i}$ observations for symmetry-related reflections.
[c] $R_{work} = \Sigma_{hkl}|F_{obs} - F_{calc}|/\,\Sigma_{hkl}|F_{obs}|$.
[d] $R_{free} = \Sigma_{hkl\ \Sigma T}|F_{obs} - F_{calc}|/\,\Sigma_{hkl}|F_{obs}|$, where the test set T includes 7% of the data.
[e] Root-mean-square deviation.

were performed until R_{free} ceased to decrease. The final models incorporated 256 of 267 possible amino acids for both structures. Residues 1–4 and 261–267 were not visible in the electron density map of any structure and were omitted from the final model. At this stage, group B-factors were refined followed by refinement of individual B-factors. Noncrystallographic symmetry (NCS) restraints (300 kcal mol^{-1} Å^{-2} in initial rounds and 50 kcal mol^{-1} Å^{-2} in the final round) between the two monomers in the dimer were used in all stages of refinement. Waters were added with the automated water-picking program in CNS using a 3.0 σ cutoff in $F_o - F_c$ maps (60 total for the phosphonatase-Mg(II) structure and 123 total for the phosphonatase-Mg(II)-vSO_3 structure). A model of vSO_3 was built in the program QUANTA (Molecular Simulations Inc.) and fit into the active site of the enzyme using a $2\,F_o - F_c$ simulated annealing omit map and a $F_o - F_c$ map. Relevant refinement statistics are given in Table I. Analysis of the Ramachandran plot of the final model showed good geometry as defined by PROCHECK (23) for both structures. Connolly (solvent accessible) surfaces were calculated using the program VOIDOO (24).

RESULTS AND DISCUSSION

Structures of Phosphonatase Complexed with Mg(II) and Mg(II) Plus vSO^3—The structures of these two phosphonatase complexes were determined to 2.8 and 2.4 Å resolution, respectively. Both structures are homodimers of 30-kDa subunits, as is the structure of the phosphonatase-Mg(II)-tungstate complex described previously (14). In each structure, both subunits contain a Mg(II) ligand. In the phosphonatase-Mg(II)-vSO_3 structure, only one of the two subunits contain the vSO_3 ligand. Occupancy of a single subunit was also observed in the phosphonatase-Mg(II)-tungstate complex, in which only one of the two subunits contained tungstate.

The phosphonatase subunit observed in the structures reported here, and in the phosphonatase-Mg(II)-tungstate complex reported previously, consists of a cap domain (residues 21–99) and a larger core domain (residues 5–20 and 100–260) (Fig. 3*A*). Both Mg(II) and vSO_3 bind to the core domain. The sulfono group of the vSO_3 binds to the same site in the core domain as tungstate (an analog of the orthophosphate product) binds in the phosphonatase-Mg(II)-tungstate complex (14). The Schiff base forming Lys-53 is located on the cap domain.

The core domain has an α/β-type structure consisting of a centrally located six-stranded antiparallel β-sheet (β4-β3-β1-β5-β6-β7) surrounded by six α-helices. The "cap domain" is inserted between the first β-strand (β1) and the first α-helix (α6) of the core domain through two flexible, solvated linker regions (residues 20–24 (L1) and 99–104 (L2). The cap domain consists of an anti-parallel, five-helix bundle. Helices α1, α3, and α4 are all approximately three-turn helices, whereas α2 and α5 are two- and five-turn helices, respectively. Helices α2 and α3 and the short loop between them point toward the core domain of the protein and form one half of the subunit interface. The residues that make up the other half of the subunit interface are positioned on loops connecting the strands of the β-sheet within the core domain.

In the published phosphonatase-Mg(II)-tungstate complex, the subunit that contains the tungstate ligand assumes a closed conformation in which the cap domain is bound to the core domain. The subunit that contains only the Mg(II), assumes an open conformation in which the cap and core domains are separated. The structure of the phosphonatase-Mg(II) complex reveals one subunit in the open conformation and one subunit in the closed conformation. This is also true of the phosphonatase-Mg(II)-vSO_3 structure, in which the subunit that contains the vSO_3 ligand is in the closed conformation. The α-carbons of the subunits of the phosphonatase-Mg(II) complex can be superimposed on those of the phosphonatase-Mg(II)-vSO_3 structure, having the same conformation (*i.e.* open or closed) with a root-mean-square deviation of 0.61 Å. Therefore, it is apparent that the vSO_3 ligand does not induce a change in backbone conformation within the core domain or cap domain.

Solution studies have indicated that vSO_3 (or tungstate) binding stabilizes the closed conformation (25). Here we observe that vSO_3 (or tungstate) binding is not necessary for formation of the closed conformation (*i.e.* both open and closed conformations are seen in the phosphonatase-Mg(II) complex); however only the closed conformation is observed when the core domain active site is complexed with ligand. Conversion of the open to the closed conformation involves the movement of the cap and core domains as "rigid bodies" with the residues of the two linkers (23–26 and 90–94) acting as a mechanical hinge

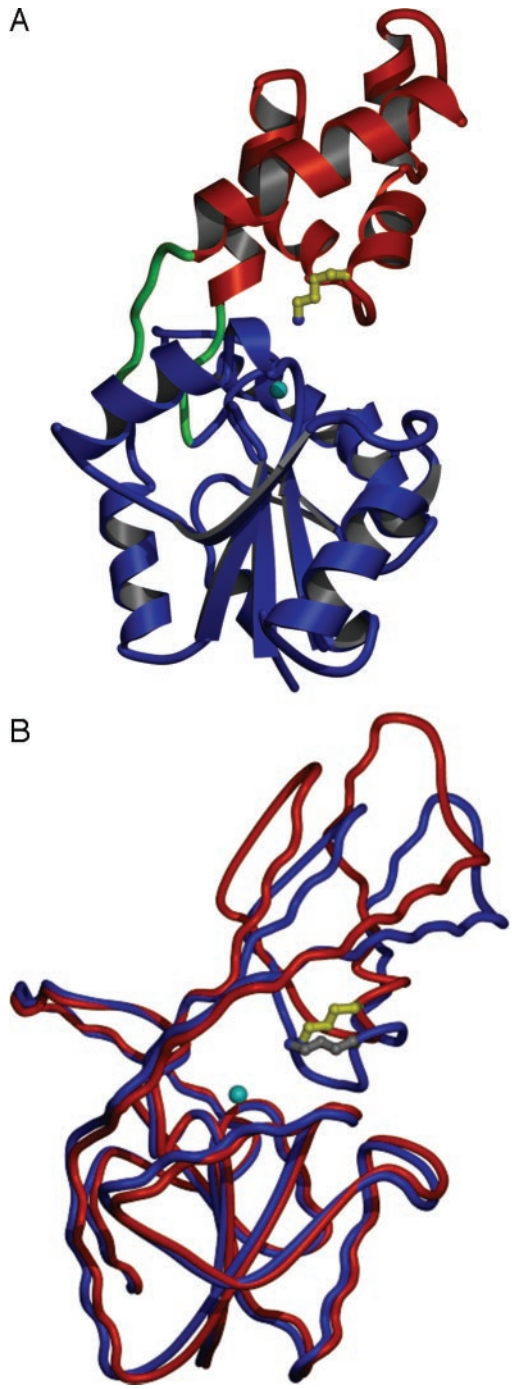

FIG. 3. **The three-dimensional structure of wild-type *B. cereus* phosphonatase (Protein Data Bank accession code 1FEZ).** *A*, ribbon diagram of the "open conformation" of the wild-type enzyme complexed with Mg(II). Coloring scheme: *red*, cap domain; *blue*, core domain; *green*, linkers; *yellow*, Lys-53; *cyan*, Mg(II). *B*, coil diagram of the overlay of the enzyme-Mg(II) complex in the open conformation (*red* backbone; *yellow*, Lys-53) and the enzyme-Mg(II)-tungstate complex in the closed conformation (*blue* backbone; *gray*, Lys-53). Mg(II) is shown in *cyan* to mark the active site.

(see Fig. 3*B*). The movement of the cap domain with respect to the core domain produces a rotation of 22° (calculated with the program DynDom (26)), resulting in a change in position of residues at the top of the cap domain by as much as 10.3Å (measured by the position of the Cα of residue 75). The difference in the backbone positions of the Schiff base-forming Lys-53 and surrounding residues is in the range of 3 to 4 Å.

The catalytically active conformation is the closed conformation. The catalytic site is formed by residues from the core and cap domains, which in turn must be associated to exclude solvent. For the open conformer, the calculated Connolly surface map delineates more than one path by which substrate and product association/dissociation can be achieved. In contrast, in the closed conformation, there is no pathway connecting the active site to bulk solvent. In fact, the only pocket large enough to accommodate solvent lies within the active site, coinciding with the binding site of the vSO_3. This result suggests that substrate binds to the open form of the enzyme and that catalysis follows conversion to the closed conformer.

Active Site Residues—The electron density map of the active site region of the phosphonatase-sulfonate-Mg(II)-vSO_3 is shown in stereo in Fig. 4*A*, and a view of the entire active site is shown in Fig. 4*B*. Importantly, two ordered, active site water molecules (Wat-111 and Wat-120) are clearly seen in the phosphonatase-Mg(II)-vSO_3 structure that were not previously observed in the structure of the phosphonatase-Mg(II)-tungstate complex (solved at 3.0 Å resolution). Two additional water molecules in the phosphonatase-Mg(II) complex replace the two sulfonate oxygens of vSO_3 ligand in the phosphonatase-Mg(II)-vSO_3 structure.

vSO_3, which competes with Pald for the core domain binding site, has a K_i = 1.79 ± 0.03 mM at pH 7.0. The phosphonatase-Mg(II)-vSO_3 complex may "roughly" resemble the Lys53-N-ethylene-Asp8-phosphate enzyme intermediate that is formed by Asp8 catalyzed dephosphonylation of the Schiff base formed between Pald and Lys53 (Fig. 1). Fig. 4*C* shows the-active site model in which Pald is substituted for the vSO_3. Because both the tungstate ligand and the sulfono group of the vSO_3 ligand occupy the same binding site, the Pald phosphonyl binding site is certain. The carbon chain of the Pald fits well into the space occupied by the vinyl group of the vSO_3 ligand and the amino acid side chains and water molecules that surround it are easily identified.

From the active site model, it can be seen that Lys53 is positioned for nucleophilic attack on the Pald carbonyl carbon and that the Pald carbonyl oxygen is within hydrogen bond distance of Wat-120. Wat-120 is also in close proximity to the Lys-53 Nϵ-amine group, the His-56 ring nitrogen, and the Met-49 sulfur atom. The functional groups of Cys-22 and Tyr-128 (and Wat-111) are peripheral to the reaction center (~6 Å from the Pald carbonyl oxygen), but they do nevertheless contribute to its microenvironment. Based on an alignment of the eight known phosphonatase sequences, His-56, Met-49, and Tyr-128 are shown to be stringently conserved, but Cys-22 is not (in seven sequences it is replaced by Ser). To evaluate their contributions to catalysis, His-56, Met-49, Cys-22, and Tyr-128 were replaced by site-directed mutagenesis.

Site-directed Mutagenesis of Potential Catalytic Groups—From previous studies, carried out with the phosphonatase from *Samonella typhimurium,* it is known that replacement of the Schiff-base-forming Lys with Arg removes all catalytic activity (*7*). *B. cereus* phosphonatase mutant proteins were purified and characterized and the catalytic constants resulting from the amino acid substitutions of residues surrounding the Lys-53 are reported in Table II. Cys-22 and Tyr-128 were mutated separately and then together. The k_{cat}/K_m for C22A was 100-fold less than that of the wild-type enzyme whereas the k_{cat}/K_m of C22S mutant was only 10-fold less. Thus, it appears that the size and polarity of the Cys-22 side chain (approximated in the C22S mutant but not in the C22A mutant) is important but not essential. The acidity of the thiol group, crucial if the residue is to function in acid/base catalysis, cannot be considered a key factor in catalysis because the C22S mutant retains 10% wild-type activity in *B. cereus* phosphona-

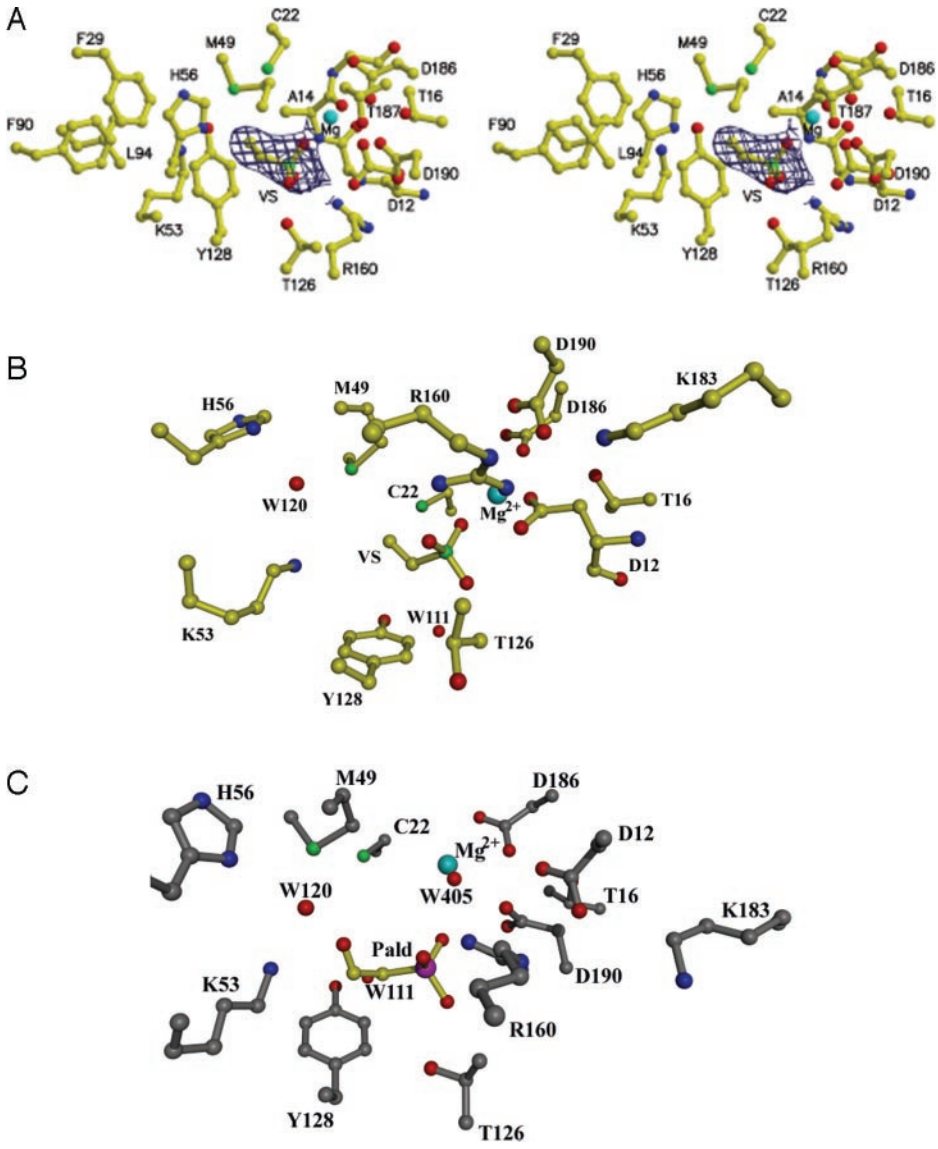

FIG. 4. *A* and *B*, active site region of the vSO_3 phosphonatase complex in stereo with the $2F_o - F_c$ electron density map (contoured at 2 σ) around the ligand depicted as *blue cages* (*A*) and showing residues surrounding both the Schiff-base lysine and Mg^{2+} cofactor (*B*). The amino acid residues are depicted in *ball-and-stick* form and the Mg^{2+} as a *cyan sphere*. *C*, the active site model generated by docking the Pald into the active site of *B*.

TABLE II

The steady-state kinetic constants for wild-type and mutant phosphonatase

Reactions contained Pald, 10 mM $MgCl_2$, 0.15 mM NADH, and 5 units/ml alcohol dehydrogenase in 50 mM K^+-Hepes (pH 7.5, 25 °C). The concentration of phosphonatase used was in the range of 0.02 to 2 μM depending on the mutant studied.

Enzyme	k_{cat}	K_m	K_{cat}/K_m
	s^{-1}	μM	$s^{-1}\ M^{-1}$
Wild type	$1.5 \pm 0.1 \times 10^{1}$	33 ± 2	5.0×10^{5}
Y128F	2.21 ± 0.02	45 ± 2	4.9×10^{4}
Y128A	$7.73 \pm .03 \times 10^{-2}$	35 ± 3	2.2×10^{3}
C22A	1.95 ± 0.04	530 ± 20	3.7×10^{3}
C22S	2.26 ± 0.09	33 ± 5	6.9×10^{4}
Y128F/C22S	2.11 ± 0.03	33 ± 2	6.4×10^{4}
H56A	$7.5 \pm 0.1 \times 10^{-2}$	145 ± 6	5.2×10^{2}
M49L	$1.5 \pm 0.1 \times 10^{-1}$	$5.1 \pm 0.3 \times 10^{3}$	2.9×10^{1}

tase and because Ser functions in place of Cys-22 in other phosphonatases.

The k_{cat}/K_m value for Y128F phosphonatase was 10-fold smaller than that of wild-type phosphonatase and the k_{cat}/K_m value for Y128A was 230-fold smaller. The space filling character of the aromatic ring, which was retained in the Y128F mutant but not in the Y128A mutant, is therefore considered to be important for efficient catalysis. The rate contribution of the side chain hydroxyl group (a factor of 10) was, however, too small to support its role in acid/base catalysis.

Interestingly, the effects of amino acid substitution at both sites were not additive. The k_{cat}/K_m of the Y128F/C22S double mutant was only 10-fold less than that of wild-type phosphonatase. We have concluded that Cys-22 and Tyr-128 (and the Wat-111 that forms a hydrogen bond to the hydroxyl of the Tyr ring) do not play important roles in catalysis, *i.e.* they do not function as acid/base catalysts.

The replacement of Met-49 with Leu resulted in a 17,000-fold reduction in k_{cat}/K_m. The space-filling property of the Met-49 side chain was retained in the M49L mutant, but the potential for interaction between the sulfur atom and Wat-120 was obviated. The replacement of His-56 with Ala and the resulting

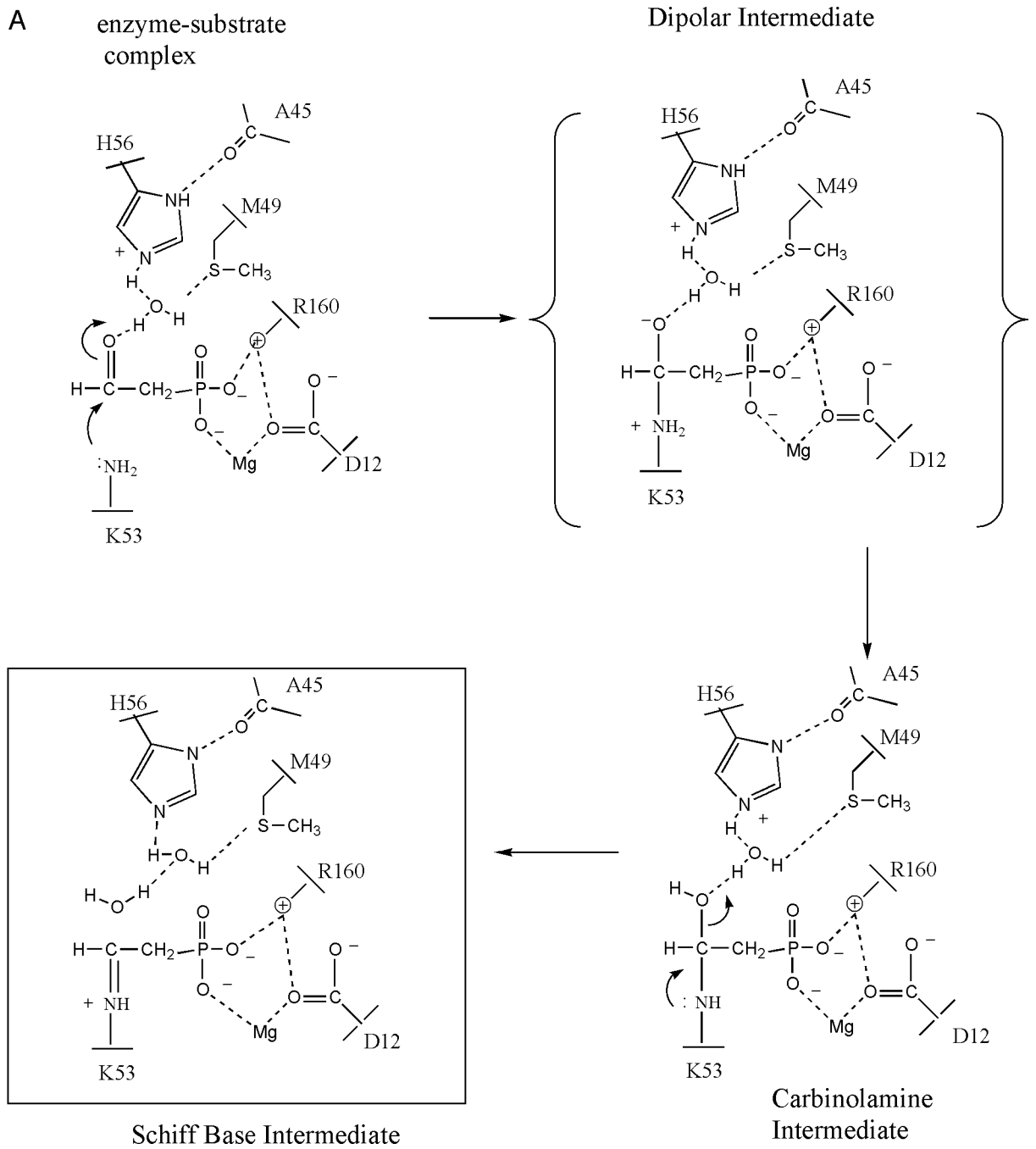

FIG. 5. **Two possible mechanisms for phosphonatase-catalyzed Schiff-base formation under consideration.** *A*, His-56 is protonated in the enzyme-substrate complex. *B*, proton is stationed on Lys-53 in the enzyme-substrate complex.

loss of acid/base and/or hydrogen-bonding function resulted in a 1000-fold reduction in k_{cat}/K_m. Thus, both His-56 and Met-49 are thought to play important roles in catalysis.

Schiff-base Formation—The structure of the phosphonatase active site with Mg(II) and modeled Pald (Fig. 4*C*) indicates that the Nϵ-amino group of Lys-53 is positioned for attack at the Pald carbonyl. Tyr-128 (with bound Wat-111) and Cys-22 are, however, too far removed from the two reacting groups to function as acid or base catalysts. Indeed, the Y128F/C22S double mutant retains 10% of the wild-type phosphonatase activity. Based on their unfavorable orientation and small rate contribution, Tyr-128 and Cys-22 were eliminated as possible acid/base catalytic groups.

There is, in fact, only a single group within hydrogen bonding distance of Lys-53 and the Pald carbonyl oxygen, and that is Wat-120. Wat-120 is also within hydrogen bonding distance of the His-56 ring nitrogen and proximal (~3.5 Å) to the Met-49 sulfur atom. Mutation of His-56 to Ala (to remove groups capable of forming hydrogen bonds) and Met-49 to Leu (to remove the sulfur group but to partially preserve the hydrophobic and space filling properties of the Met side chain) resulted in significant losses (1,000- and 17,000-fold, respectively) in catalytic efficiency. Thus, based on their favorable positioning within the active site and on their large rate contribution, these two residues were judged to play important roles in catalysis of Schiff-base formation.

Two mechanisms for Schiff-base formation consistent with these results are illustrated in Fig. 5. The mechanism presented in Fig. 5*A* will be discussed first. As the cap domain closes over the core domain (see Fig. 2*B*), His-56, Lys-53, and

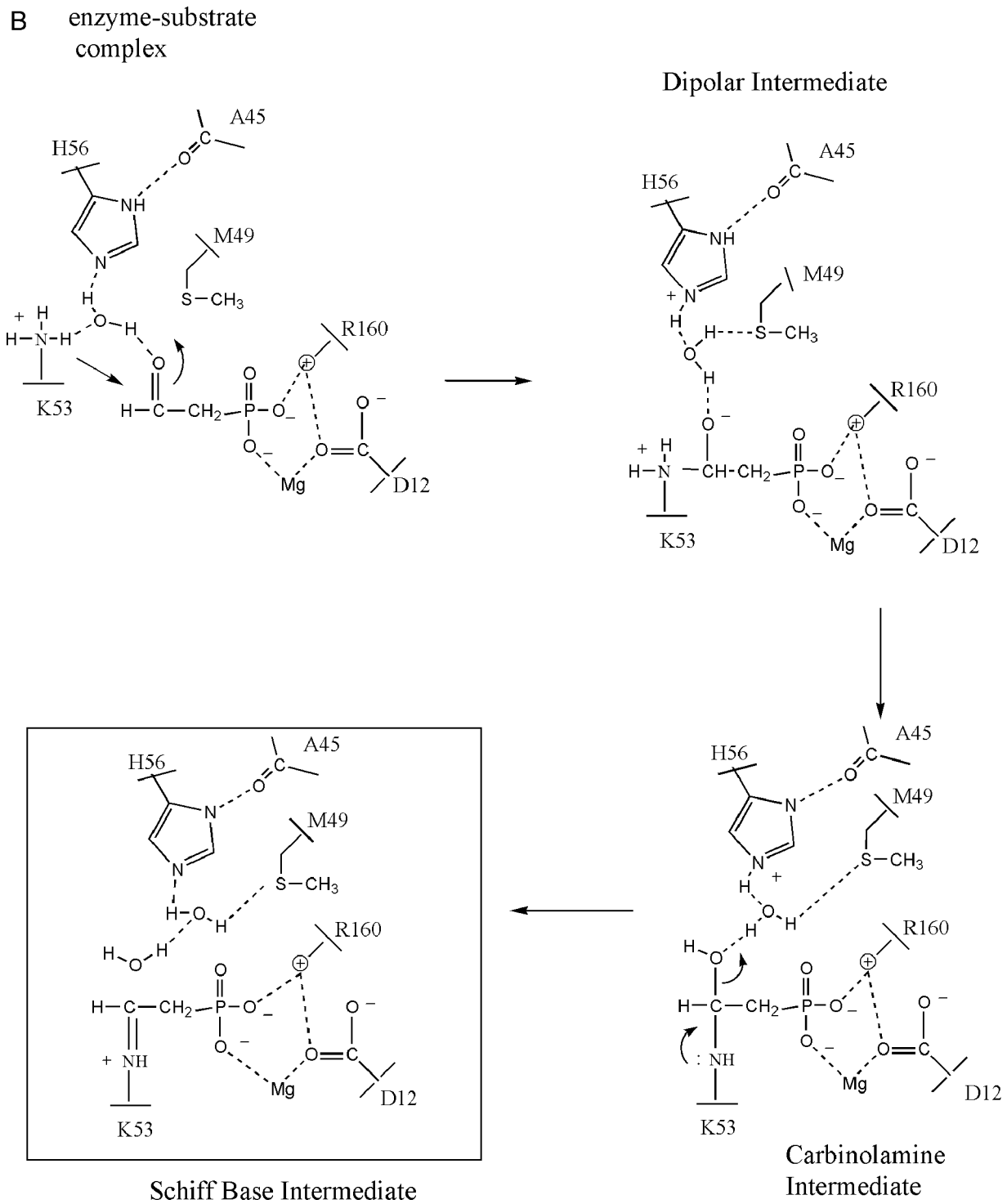

FIG. 5—*continued*

Met-49 are removed from bulk solvent and placed into the active site of the core domain where Pald and Mg(II) are bound. The charged Lys-53 Nϵ-ammonium group (pK_a = 9.3 in open enzyme conformer (25)) may lose a proton to His-56 to which it is connected via the bridging Wat-120. The pK_a difference in the solvated Lys-53 and His-56 may be reduced by the active site environment, with the proton stabilized on the His-56 ring and not on the Lys-53 nitrogen (see below). The Wat-120 forms a hydrogen bond with the Pald carbonyl and with the Met-49 sulfur atom, thus extending the hydrogen bond network that originates from His-56.

The attack of the neutral Lys-53 at the substrate carbonyl produces the dipolar intermediate described earlier (see Fig. 5). Spontaneous proton movement from nitrogen to oxygen generates the carbinolamine intermediate. Proton transfer from the protonated His-56 to the hydroxide-leaving group of the carbinolamine via Wat-120 accompanies Schiff-base formation. The protonated Schiff-base will serve as the electron sink in the ensuing attack of the Asp-12 carboxylate on the phosphonyl phosphorus (Fig. 1).

An alternate and kinetically equivalent route to the dipolar intermediate is shown in Fig. 5*B*. Here, the reaction begins from an active site configuration in which the Lys-53, rather than the His-56, is protonated. Wat-120 would function as

general base, deprotonating the Lys-53 as it attacks the Pald carbonyl.

Phosphonatase shares the use of electrophilic catalysis by Schiff-base formation with numerous C–C bond-cleaving enzymes including acetoacetate decarboxylase, transaldolase, and Class I aldolases (for review see Ref. 8). How do the mechanisms proposed for Schiff-base formation in phosphonatase compare with those of the C–C bond lyases? For instance, acetoacetate decarboxylase (27–29) and fructose (bis)phosphate aldolase (30–32) employ electrostatic forces to destabilize the protonated Lys Nϵ-amino group. Adjacent to the Schiff-base-forming Lys residue resides a more basic Lys (positioned in a polar environment that favors the ammonium form of the amine). Because of charge-charge repulsion, only the more basic of the two Lys residues will be protonated at physiological pH. Thus, the Schiff-base-forming Lys will be neutral and able to function as a nucleophile.

The Lys-53 of phosphonatase is located at the N terminus of an α-helix where it is placed under the influence of the positive pole of the helix macrodipole. In the open conformer, where the Lys-53 is solvated, the pK_a of the Lys is reduced from the expected value of 10.5 (33) to 9.3 (25). In the closed conformation, wherein nonpolar side chains surround Lys-53, the positive charge on the Nϵ will be further destabilized. The proton may be more effectively accommodated on the neighboring basic residue, *i.e.* His-56. Environmental factors, *e.g.* the microenvironment and the extensive hydrogen bond network that incorporates the proton on the His-56 ring (comprising the ring N(1)H of the His-56, the backbone carbonyl of Ala-45, the N(3)H hydrogen bond to Wat-120, and the hydrogen bond between Wat-120 and the sulfur atom of Met-49) may serve to increase the basicity of His-56 to a value greater than that of Lys-53 when the enzyme is in the closed conformation. Consequently, at neutral pH (Fig. 5*A*), which is both the pH optimum for catalysis (34) and the prevailing pH in the cell, His-56 is charged and Lys-53 is not.

The alternate catalytic strategy (depicted in Fig. 5*B*) requires His-56 to be neutral and, through the hydrogen-bonded Wat-120, to act as a general base for removal of the proton from the Nϵ-ammonium group of the Lys-53 as it approaches the substrate carbonyl. This mechanism is similar to those used by D-2-deoxyribose-5-phosphate aldolase (35) and 2-keto-3-deoxy-6-phosphogluconate aldolase (36). These enzymes utilize an aspartate-bound water and a glutamate, respectively, to deprotonate the Schiff-base-forming lysine.

An interesting distinction between the catalytic strategies of phosphonatase and the Class I aldolases is in the selection of the acid group used to deliver a proton to the hydroxy group of the carbinolamine intermediate. D-2-Deoxyribose-5-phosphate aldolase (35), 2-keto-3-deoxy-6-phosphogluconate aldolase (36), fructose 1,6-(bis)phosphate aldolase (30–32), and transaldolase (37) employ a protonated glutamate or aspartate residue (either directly or via a bridging water molecule) as acid catalyst in the dehydration of the carbinolamine. In contrast, the phosphonatase Asp-12, which is positioned for backside, in-line attack at the phosphonyl group of the Schiff-base intermediate, is not positioned to protonate the carbinolamine hydroxyl group as is required for catalysis of the preceding dehydration step. Thus, in phosphonatase, acid catalysis is performed by His-56–Wat-120, whereas nucleophilic catalysis is achieved with Asp-12, located some distance from the Lys-53-Pald carbonyl reaction center.

Conclusions—The x-ray crystallographic structure determinations of the phosphonatase-Mg(II) and phosphonatase-Mg(II)-vinylsulfonate complexes reported here and the phosphonatase-Mg(II)-tungstate reported earlier (14) show that phosphonatase can exist in a cap domain-core domain open conformation and in a cap domain-core domain closed conformation. The conformer interconversion occurs through movement in the hinge region of the solvated interdomain linkers. In the open conformation, the cap and core domains are separated to allow solvent access to the active site of the core domain. In this conformation, the enzyme can bind substrate and release product. The closed conformation is required for catalysis. In this conformation, the cap and core domains are bound, thereby sealing the active site from solvent. In addition, it is in the closed conformation that three essential residues from the cap domain are positioned within the active site of the core domain. These residues include the Schiff-base-forming Lys-53 and the two residues (Met-49 and His-56) that bind Wat-120. Wat-120 is positioned for proton relay to and from the reaction center. The electrostatic environment of the active site of the closed conformer appears to stabilize the protonated ring of His-56 and destabilize the protonated ammonium group of Lys-53. It is therefore tempting to propose a mechanism of catalysis in which a proton is transferred from the Lys-53 to His-56 upon domain-domain closure. This transfer facilitates nucleophilic attack of the Lys-53 nucleophilic attack on the Pald carbonyl carbon and protonation of the carbonyl oxygen via the His-56—Wat-120 dyad. The composite picture of Schiff base formation in phosphonatase is unique. It represents yet another answer to the problem of catalysis of Schiff base formation, which is not available to the solution reaction.

Acknowledgment—We thank Brookhaven National Laboratory's National Synchrotron Light Source for use of beamline X12B for data collection.

REFERENCES

1. Kononova, S. V., and Nesmeyanova, M. A. (2002) *Biochemistry* (*Mosc.*) **67,** 184–195
2. Wackett, L. P., Shames, S. L., Venditti, C. P., and Walsh, C. T. (1987) *J. Bacteriol.* **169,** 710–717
3. McMullan, G., and Quinn, J. P. (1994) *J. Bacteriol.* **176,** 320–324
4. Ternan, N. G., and Quinn, J. P. (1998) *Biochem. Biophys. Res. Commun.* **248,** 378–381
5. La Nauze, J. M., Rosenberg, H., and Shaw, D. C. (1970) *Biochim. Biophys. Acta* **212,** 332–350
6. Olsen, D. B., Hepburn, T. W., Moos, M., Mariano, P. S., and Dunaway-Mariano, D. (1988) *Biochemistry* **27,** 2229–2234
7. Baker, A. S., Ciocci, M. J., Metcalf, W. W., Kim, J., Babbitt, P. C., Wanner, B. L., Martin, B. M., and Dunaway-Mariano, D. (1998) *Biochemistry* **37,** 9305–9315
8. Allen, K. N. (1998) in *Comprehensive Biological Catalysis* (Sinnot, M., ed) pp. 135–172, Academic Press, New York
9. Guthrie, J. P. (1972) *J. Am. Chem. Soc.* **94,** 7024–7029
10. Guthrie, J. P., and Westheimer, F. H. (1967) *Fed. Proc.* **26,** 562
11. Marion H. O'Leary, and Baughn, R. L. (1972) *J. Am. Chem. Soc.* **94,** 626–630
12. Jencks, W. P. (1969) *Catalysis in Chemistry and Enzymology*, pp. 121–122, McGraw Hill Inc., New York
13. Isbell, A. F., Englert, L. F., and Rosenberg, H. (1969) *J. Org. Chem.* **34,** 755–756
14. Morais, M. C., Zhang, W., Baker, A. S., Zhang, G., Dunaway-Mariano, D., and Allen, K. N. (2000) *Biochemistry* **39,** 10385–10396
15. Bradford, M. M. (1976) *Anal. Biochem.* **72,** 248–254
16. Morais, M. C., Baker, A. S., Dunaway-Mariano, D., and Allen, K. N. (2000) *Acta Crystallogr. Sect. D. Biol. Crystallogr.* **56,** 206–209
17. Otwinowski, Z., and Minor, W. (1997) *Methods Enzymol.* **276,** 307–326
18. Matthews, B. W. (1985) *Methods Enzymol.* **114,** 176–187
19. Rossmann, M. G. (1990) *Acta Crystallogr. Sect. A.* **46,** 73–82
20. Navaza, J. (2001) *Acta Crystallogr. Sect. D. Biol. Crystallogr.* **57,** 1367–1372
21. Brunger, A. T. (1992) *Nature* **355,** 472–474
22. Jones, T. A., Zou, J. Y., Cowan, S. W., and Kjeldgaard. (1991) *Acta Crystallogr. Sect. A* **47,** 110–119
23. Laskowski, R. A., MacArthur, M. W., Moss, D. S., and Thornton, J. M. (1993) *J. Appl. Crystallogr.* **26,** 283–291
24. Kleywegt, G. J., and Jones, T. A. (1994) *Acta Crystallogr. Sect. D. Biol. Crystallogr.* **50,** 178–185
25. Zhang, G., Mazurkie, A. S., Dunaway-Mariano, D., and Allen, K. N. (2002) *Biochemistry* **41,** 13370–13377
26. Collaborative Computational Project Number 4 (1994) *Acta Crystallogr. Sect. D. Biol. Crystallogr.* **50,** 760–768
27. Schmidt, D. E., Jr., and Westheimer, F. H. (1971) *Biochemistry* **10,** 1249–1253
28. Kokesh, F. C., and Westheimer, F. H. (1971) *J. Am. Chem. Soc.* **93,** 7270–7274
29. Highbarger, L. A., Gerlt, J. A., and Kenyon, G. L. (1996) *Biochemistry* **35,** 41–46
30. Maurady, A., Zdanov, A., de Moissac, D., Beaudry, D., and Sygusch, J. (2002) *J. Biol. Chem.* **277,** 9474–9483

31. Choi, K. H., Mazurkie, A. S., Morris, A. J., Utheza, D., Tolan, D. R., and Allen, K. N. (1999) *Biochemistry* **38,** 12655–12664
32. Choi, K. H., Shi, J., Hopkins, C. E., Tolan, D. R., and Allen, K. N. (2001) *Biochemistry* **40,** 13868–13875
33. Voet, D., and Voet, J. G. (1990) *Biochemistry*, p. 62, John Wiley & Sons, New York
34. Olsen, D. B., Hepburn, T. W., Lee, S. L., Martin, B. M., Mariano, P. S., and Dunaway-Mariano, D. (1992) *Arch. Biochem. Biophys.* **296,** 144–151
35. Heine, A., DeSantis, G., Luz, J. G., Mitchell, M., Wong, C. H., and Wilson, I. A. (2001) *Science* **294,** 369–374
36. Allard, J., Grochulski, P., and Sygusch, J. (2001) *Proc. Natl. Acad. Sci. U. S. A.* **98,** 3679–3684
37. Jia, J., Schorken, U., Lindqvist, Y., Sprenger, G. A., and Schneider, G. (1997) *Protein Sci.* **6,** 119–124